Cross sections for the electron-impact excitations $\tilde{A}^1B_1$ and $\tilde{B}^1A_1$ of H_2O determined by high-energy electron scattering

Wei-Qing Xu,[2,*] Zi-Ru Ma,[1,*] Yi-Geng Peng,[3,4,*] Xiao-Jiao Du,[1] Yuan-Chen Xu,[1] Li-Han Wang,[1] Bo Li,[1] Hao-Ran Zhang ⓞ,[1] Bei-Yuan Zhang ⓞ,[1] Jian-Hui Zhu,[1] Shu-Xing Wang,[1] Yong Wu,[4,†] Jian-Guo Wang,[4] and Lin-Fan Zhu ⓞ[1,‡]

[1]*Hefei National Laboratory for Physical Sciences at Microscale and Department of Modern Physics, University of Science and Technology of China, Hefei, Anhui 230026, China*
[2]*School of Physical Science and Technology, ShanghaiTech University, Shanghai 201210, China*
[3]*Department of Applied Physics, Nanjing University of Science and Technology, Nanjing 210094, China*
[4]*Institute of Applied Physics and Computational Mathematics, Beijing 100088, China*

Understanding the role of inelastic electron scattering in water is of fundamental importance in various fields ranging from atmospheric chemistry to radiation biology. The lack of accurate excitation cross sections for water results in a large uncertainty, for example, in the track structure simulation for modeling radiation damage to DNA. The large differences of the integral cross sections (ICSs) for the optical-allowed excitations $\tilde{A}^1B_1$ and $\tilde{B}^1A_1$ of H_2O among experiments and theories have been maintaining for decades. To resolve this issue, by combining the *ab initio* calculation with the electron correlation being taken into account accurately, we compare the ICSs determined by high-energy electron scattering with the existing experiments at low and intermediate energies and theories, where the present experiment eliminated the errors from the spectral deconvolution in low-energy measurements. Our work provides a recommendation for the ICSs of the two excitations from thresholds up to several keV, and suggests the existing selected ICSs for H_2O be revised for accurate modeling radiation effects in biological matter and describing the transport properties of electrons in aqueous systems.

I. INTRODUCTION

Interactions between electrons and water are an extremely attractive subject in a variety of scientific areas, including atmospheric and interstellar chemistry, radiation physics, and chemistry, radiation biology and medicine [1–8]. For instance, the reliable radiation track simulation in biological tissue mainly composed of water, to model radiation damage leading to hydrated DNA breakup [5], has been limited by the lack of the accurate and complete electron scattering cross sections for liquid water in the keV-scale range [7–14]. Therefore the experimental data of vapor water [6–9,11,15] and ice [16] are extrapolated to the unit density environment of the liquid and used in various models. Electronic excitation is one of the significant energy deposition channels, while its cross sections for water are differed among different theoretical approaches and semi-empirical models within the framework of the first Born approximation (FBA) [7–13,17], especially at low electron impact energies ($E_0 <\sim 100$ eV). Therefore the accurate and complete experimental excitation cross sections for H_2O, which can evaluate the theoretical methods and can be used directly, are the prerequisite for the accurate radiation track simulation.

Differential and integral cross sections (DCSs, ICSs) for electron-impact excitations of low-lying electronic states in

H_2O have been extensively investigated both experimentally [13,17–28] and theoretically [19,20,29–39], however, remain a very poor agreement among them. Experimentally, a number of optically forbidden transitions vastly contribute to excitation processes at low electron energies ($E_0 \lesssim 100$ eV) [18–23,27,28], leading to the heavily spectral overlapping of electronic excitations in H_2O, which may result in serious spectral fitting errors in the extraction of DCSs and ICSs [18–23,27,28]. Moreover, the existing elastic DCSs of H_2O, showing a largely quantitative disagreement among different measurements and calculations [40], are usually used to normalize excitation DCSs on an absolute scale, which may introduce more errors into the experimental results [19–26]. On the theoretical side, due to a strong permanent dipole moment (1.85D) and a significant mean dipole polarizability ($9.79a_0^3$) of polar molecule H_2O [13], an accurate description for the target states is nontrivial, which makes it a very hard challenge for current state-of-the-art scattering calculations [19,20,29–38], for example, the calculation of the excitation cross sections considering the multichannel coupling is a very difficult task [41]. To include the long-range nature of the electron-dipole interaction, the procedure using Born closure formula [42] is often employed to obtain the DCS for high partial waves in the FBA, and which is added to that for the low partial waves (short-range interaction) in the fixed-nuclei approximation (FNA) [19,20,29–38]. Here difficulties arise from the nonconvergence of the partial wave expansion in the FNA. Beyond the FNA, a *R*-matrix calculation on the ICSs for the excited states $^{3,1}B_1$ and $^{3,1}A_1$ of H_2O within the adiabatic-nuclei

*These authors contributed equally to this work.
†wu_yong@iapcm.ac.cn
‡lfzhu@ustc.edu.cn

approximation (ANA) includes the effects of one-dimensional nuclear motion away from the ground state equilibrium geometry [30]. However, the significant differences with the previous experiments [18–23] and theories [19,20,29] still exist in both magnitude and profile. Furthermore, the mixed valence-Rydberg character of low-lying electronic states of H_2O is particularly difficult to be depicted with single-configuration wave functions [19,20,33,34,36,38]. Consequently, the big disagreement among theories and experiments can not be unambiguously resolved, which makes the comparison inconclusive.

In this paper, we report the ICSs for the electronic states $\tilde{A}^1B_1$ and $\tilde{B}^1A_1$ of H_2O using high-energy electron scattering for eliminating the errors from the spectral deconvolution in low-energy experiments and from the absolute normalization procedure. This work explored the dramatic discrepancies of the ICSs among earlier experiments and theories for decades by combining the present *ab initio* calculations, and the purpose is to provide a recommendation for ICSs in the keV-scale range.

II. EXPERIMENTAL APPARATUS AND PROCEDURES

The experimental apparatus has been described elsewhere [43], which mainly consists of a thermionic electron gun, two hemispherical energy selectors, and cylindrical electrostatic optics. The electron energy was set at 1500 eV with an energy resolution of about 70 meV (FWHM), and the background pressure in the collision chamber was around 5×10^{-5} Pa. The electron energy-loss spectra in the angular range of $1.5°$–$9.0°$ with an angular resolution of about $0.8°$ (FWHM) were measured, and the angular intervals are $0.5°$ for $1.5°$–$5.5°$ and $1.0°$ for $6°$–$9°$, respectively. The standard relative flow technique [44] was utilized to determine absolute DCSs for electronic excitations of H_2O. Gaseous sample (H_2O) was degassed by a repeated freeze-pump-thaw cycle from high purity distilled water. The mixed H_2O and helium with the same flow rates of 0.7 sccm for the angles $<5°$ and 1.0 sccm for the rest angles set by a MKS vapor source mass flow controller (MFC) 1150C and a normal MFC (Beijing Sevenstar CS200), respectively, were leaked into the collision chamber simultaneously and continuously. For the gas path of water vapor, a positive temperature gradient was maintained on the components and plumbing from the source cell ($\sim$40 °C), and MFC 1150C (50 °C) to the collision chamber ($\sim$70 °C) to prevent condensation. Noticeable nonlinear change of the spectral signals for H_2O vs flow rates was not observed, which indicates water clusters and double scattering are absent at present flow rates (pressure inside chamber $<5 \times 10^{-3}$ Pa).

The DCS $d\sigma_{H_2O}/d\Omega$ of a specified excitation with an excitation energy E_n of H_2O can be determined from the measured electron-energy-loss spectrum (EELS) by referring to the DCS $d\sigma_{He}/d\Omega$ of $1s^2\,^1S_0 \to 1s2p\,^1P_1$ (E_{2p}) of He at a scattering angle θ [44]

$$\frac{d\sigma_{H_2O}(E_n, \theta)}{d\Omega} = \frac{\dot{n}_{He}}{\dot{n}_{H_2O}} \sqrt{\frac{M_{He}}{M_{H_2O}}} \frac{N_{H_2O}(E_n, \theta)}{N_{He}(E_{2p}, \theta)} \frac{d\sigma_{He}(E_{2p}, \theta)}{d\Omega},$$
(1)

here $\dot{n}$ represents the flow rate, and N refers to the intensity of the corresponding excitation. M is the molecular mass for the specified molecule. The $d\sigma_{He}(E_{2p}, \theta)/d\Omega$ of He has been benchmarked with a high accuracy [45]. The true zero angle was calibrated by the symmetry of the angular distribution of the inelastic scattering signals of the $1s^2 \to 1s2p$ of He around the geometry nominal $0°$.

According to the FBA, the generalized oscillator strength (GOS) can be written as (in atomic units) [46]

$$f(E_n, \mathbf{K}) = \frac{E_n}{2} \frac{p_0}{p_a} K^2 \frac{d\sigma(E_n, \theta)}{d\Omega}.$$
(2)

Here, p_0 and p_a are the incident and scattered electron momenta, respectively, and $\mathbf{K}$ is the corresponding momentum transfer vector at θ.

In addition, according to the analytic properties of GOS identified by Lassettre and his coworkers [47,48], the GOS can be represented by [47–50]

$$f(E_n, \mathbf{K}) = \frac{x^M}{(1+x)^{l+l'+M+5}} \sum_{m=0}^{\infty} \frac{f_m x^m}{(1+x)^m},$$
(3)

where $x = K^2/\alpha^2$ with $\alpha = (2I)^{1/2} + [2(I - E_n)]^{1/2}$, and I is the ionization energy. l and l' are the orbital angular momenta of the initial and final states of the target electron, while M is an integer which is relevant to the transition multipolarity [49,50] and f_m are the fitting parameters. For a dipole-allowed transition, M=0 and f_0 is the optical oscillator strength (OOS). Since the ionization energy I of an electron in a molecule is defined only in the context of a simply independent particle model by Lassettre [47], it is better to simply take α^2 as a fitting parameter along with f_m as proposed by Kim [51]. Moreover, the following function $g(x)$ with two fitting parameters a and b, in addition to the leading fraction in Eq. (3), can well represent the experimental GOS:

$$g(x) = axe^{-bx}.$$
(4)

Similar treatments can be found in the previous works [52].

From the fitted GOS results using the Lassettre formula [47–50], the Born ICSs for the electron-impact excitations can be calculated (in atomic units) [46]:

$$\sigma_{Born}(E_0) = \frac{\pi}{E_0 E_n} \int_{K_{min}^2}^{K_{max}^2} \frac{f(E_n, \mathbf{K})}{K^2} dK^2,$$
(5)

with

$$K_{min}^2 = [\sqrt{2E_0} - \sqrt{2(E_0 - E_n)}]^2$$

and

$$K_{max}^2 = [\sqrt{2E_0} + \sqrt{2(E_0 - E_n)}]^2,$$

where K_{min} and K_{max} represent the minimum and maximum momentum transfers, respectively. However, σ_{Born} is generally overestimated at low and intermediate energies [17]. Therefore Kim developed a BE-scaling approach to scale σ_{Born} into the BE-scaled ICS [17,51,53]

$$\sigma_{BE}(E_0) = \frac{E_0}{E_0 + B + E_n} \sigma_{Born}(E_0),$$
(6)

which can correct the deficiency of the FBA at low E_0, without losing its well-known validity at high E_0. Here, B is the
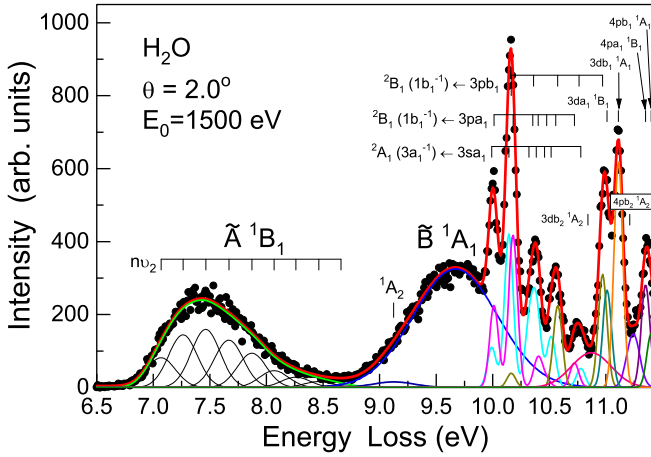
FIG. 1. A typical EELS of H_2O at an incident electron energy of 1500 eV and a scattering angle of 2.0°. Solid lines are the fitted curves (see text for details).

binding energy. The reliability of this method and the high accuracy of σ_{BE} have been widely testified by numerous experiments and theories [17,51,53].

Figure 1 shows a typical EELS of H_2O at $E_0 = 1500$ eV and $\theta = 2.0°$ with spectroscopic assignments according to Refs. [13,54,55], where the only dipole-forbidden transition observed is the $^1A_2$ at ~9.1 eV in the energy range of 6.5–10.7 eV. This makes the extraction of the contributions of $\tilde{A}^1B_1$ and $\tilde{B}^1A_1$ simple, which resolves the crux of the spectral fitting in low-energy measurements mentioned above and fundamentally improves the accuracy of the data greatly. To depict the asymmetry of $\tilde{A}^1B_1$, nine Gaussian functions were used to fit and obtain the spectral intensity, where the corresponding energy positions of the individual functions were fixed to the ones in Table 1 of Ref. [54]. $\tilde{B}^1A_1$ was reproduced by one Gaussian function, imitating Ref. [56]. The other electronic states in higher energy region were also described with Gaussian functions, and will be considered in a future paper.

Because the exact values of the energy position E_n and width $\Delta E = 2.355\sigma$ (σ is the standard deviation of a Gaussian function to describe an electronic state) for $^1A_2$ are not well known, to obtain the contributions of $\tilde{A}^1B_1$ and $\tilde{B}^1A_1$ shown in Fig. 1, the key is to determine the spectroscopic parameters of $\tilde{B}^1A_1$ and $^1A_2$. First we convoluted the high-resolution photoabsorption spectrum of Mato *et al.* shown in Fig. 1 of Ref. [54] with our experimental energy resolution (FWHM = 70 meV), and then fitted it with the similar fitting model mentioned above, but without $^1A_2$ here. The resulted parameters of $\tilde{B}^1A_1$ are $E_n = 9.67$ eV, $\Delta E = 0.88$ eV, which are in good agreement with the ones of Ralphs *et al.* ($E_n = 9.67$ eV, $\Delta E = 0.90$ eV) [19].

Next we fitted our EELSs with the fixed spectroscopic parameters of $\tilde{B}^1A_1$ obtained above in large momentum transfer range, where the intensities of $^1A_2$ are strong enough to give good fittings. Then we averaged the determined spectroscopic parameters of $^1A_2$, and finally the resulted parameters of $^1A_2$ are $E_n = 9.12$ eV, $\Delta E = 0.43$ eV, which are in good agreement with the ones of Ralphs *et al.* ($E_n = 9.20$ eV, $\Delta E = 0.38$ eV) [19]. Finally, we refitted all EELSs with the

fixed spectroscopic parameters of $^1A_2$ and $\tilde{B}^1A_1$ by the fitting model, and then the corresponding contributions for all electronic states were obtained.

The experimental errors of the GOSs in this work include the contributions from the finite angular resolution, the angle determination, the statistical counts, the fitting procedure, and the normalizing procedure, and the total experimental errors, which are shown in the corresponding figures in the following sections, are less than 15% for most data points with the ones at large angles being about 23%.

III. THEORETICAL METHOD

To perform the inelastic electron-H_2O scattering calculation for the DCSs and GOSs of $\tilde{A}^1B_1$ and $\tilde{B}^1A_1$ of H_2O in the FBA, the multireference single- and double-excitation configuration interaction method (MRD-CI) has been applied to calculate the adiabatic potential curves and wave functions of the ground and excited states based on the Born-Oppenheimer approximation [57], which accurately deals with the influence of electron correlation on the related wave functions. The electron-impact DCS $d\sigma/d\Omega$ for a specified excitation from an initial state i to a final state f of an atom or a molecule within the FBA is [17,46,58]

$$\frac{d\sigma}{d\Omega} = \frac{p_a}{p_0}|f_{B1}|^2, \quad (7)$$

here f_{B1} is the first Born scattering amplitude. For electron-molecule collision,

$$f_{B1} = -\frac{2}{K^2}\Big[F_{fi}(\mathbf{K}) - \delta_{fi}\sum_\alpha Z_\alpha e^{i\mathbf{K}\cdot\mathbf{R}_\alpha}\Big], \quad (8)$$

with

$$F_{fi}(\mathbf{K}) = \langle f|\sum_j e^{i\mathbf{K}\cdot\mathbf{r}_j}|i\rangle. $$

Here, Z_α and $\mathbf{R}_\alpha$ are the nuclear charge and the position vector of the αth atom in the molecule target, respectively. F_{fi} is called the Born amplitude, and $\mathbf{r}_j$ is the position vector of the jth electron. δ_{fi} is the usual Kronecker symbol.

For the molecule target with free spatial orientation of molecular axis in a practical experiment, the $d\sigma/d\Omega$ should be averaged by holding the molecular axis fixed and allowing $\mathbf{K}$ to change its relative orientation

$$\frac{d\bar{\sigma}(\mathbf{K})}{d\Omega} = \frac{1}{4\pi}\int\frac{d\sigma(\mathbf{K})}{d\Omega}d\Omega_{\hat{K}}. \quad (9)$$

Then by integrating the DCS numerically over the entire solid angular space, the ICS at an incident electron energy $E_0 = p_0^2/2$ is finally obtained.

Here two factors, i.e., (**1**) the accuracy of the target wave function and (**2**) the effect of the one-dimensional nuclear vibration, which affect the theoretical calculations of DCSs or GOSs for $\tilde{A}^1B_1$ and $\tilde{B}^1A_1$ of H_2O, have been clarified and concluded in the following discussion.

Taking $\tilde{X}\,^1A_1 \to \tilde{A}\,^1B_1$ as an example, note that the HOH bending- and the OH symmetrical stretching- motions are limited on the potential surfaces of $\tilde{X}$ and $\tilde{A}$, respectively, we made one OH bond stretching with the fixed HOH angle (104.5°) and another OH bond length (1.8a_0) at the
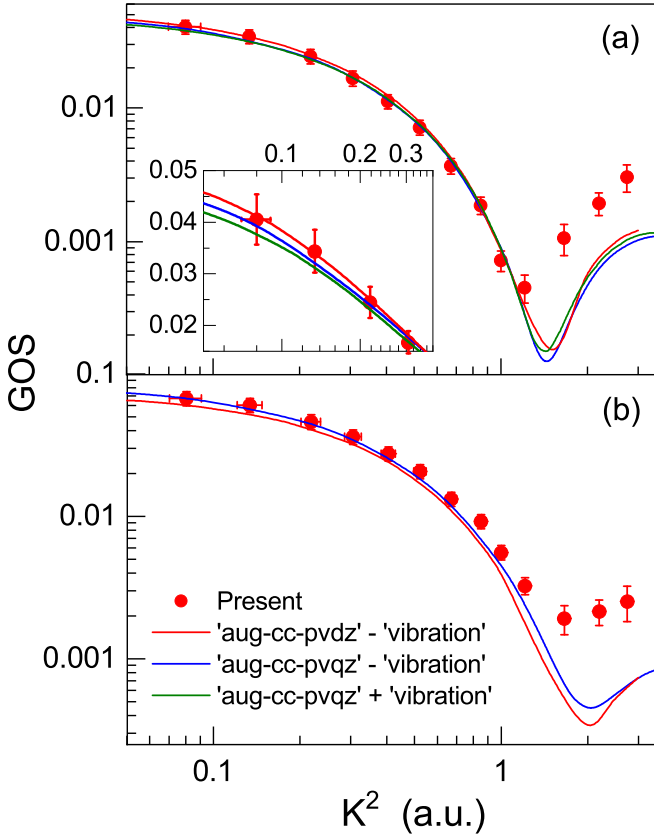
FIG. 2. The GOSs for (a) $\tilde{A}^1B_1$ and (b) $\tilde{B}^1A_1$ of H_2O compared with different modeling calculations (see text for details).

FIG. 3. The ICSs for (a) $\tilde{A}^1B_1$ and (b) $\tilde{B}^1A_1$ of H_2O compared with the present calculations (see text for details).

ground state equilibrium geometry for modeling the one-dimensional nuclear vibration. The electronic wave functions of the initial and final states were calculated with a combined MCSCF + MRD-CI approach. The Dunning's 4 zeta basis (aug-cc-pvqz) [59] were set on each hydrogen and oxygen atom. The molecular orbits were optimized with the MCSCF method embedded in the MOLPRO package [60,61], and the core shell of oxygen was kept closed and the active space was formed with the rest eight valence electrons on six active orbits. In the MRD-CI calculation [62–64], a set of configurations were selected as the reference and the final CI space were formed by single and double excitation on the reference space.

Figure 2 shows the experimental GOSs for $\tilde{A}^1B_1$ and $\tilde{B}^1A_1$ of H_2O along with different modeling calculations. The differences of the calculated GOSs for each state at different basis sets (aug-cc-pvdz and aug-cc-pvqz), and with or without the one-dimensional nuclear vibration ("+, " "−") are very small within the FBA. Due to the complex adiabatic interactions in $\tilde{B}^1A_1$, it is hard to estimate the contribution from the one-dimensional nuclear vibration here, but being reasonably neglected according to the case of $\tilde{A}^1B_1$. So the present calculations are convergent for different basis sets, and the effects from the one-dimensional nuclear vibration are ignored for both electronic states. Then the GOSs with "aug-cc-pvqz"-"vibration" are chosen as the present theoretical results for both electronic states to compare with the previous results in Sec. IV.
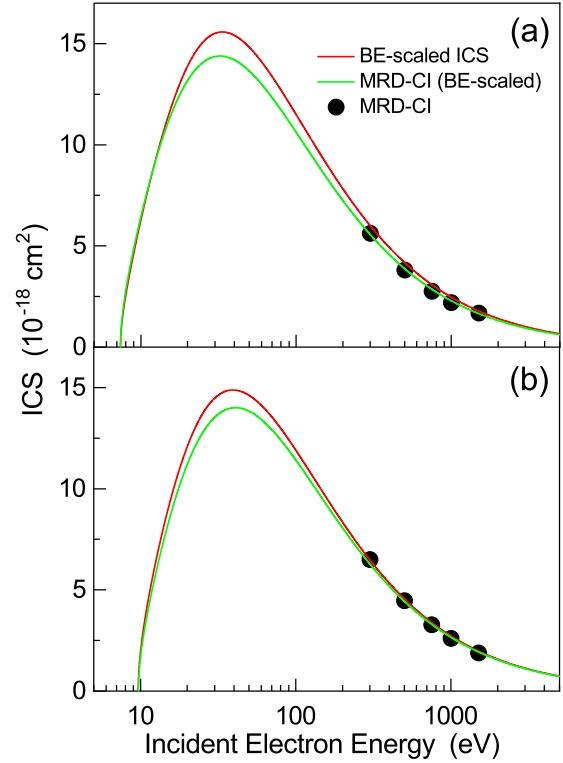
Figure 3 shows the present BE-scaled ICSs for $\tilde{A}^1B_1$ and $\tilde{B}^1A_1$ of H_2O together with the MRD-CI calculations. The "MRD-CI (BE-scaled)" results shown in Fig. 3 were obtained by integrating the corresponding GOSs (shown in Fig. 2) over K following with the BE-scaling approach with Eqs. (3)–(6). The present BE-scaled ICSs are in good agreement with "MRD-CI (BE-scaled)" ones for both electronic states over the whole energy range (the max differences at top points are less than 8% for both states) shown in Fig. 3. To confirm the present "MRD-CI (BE-scaled)" results, five data points (labled as "MRD-CI") in the energy range of 300–1500 eV were calculated by MRD-CI within the FBA. It is shown in Fig. 3 that the calculated ICS data points are in excellent agreement with the "MRD-CI (BE-scaled)" results at $E_0 \geqslant 300$ eV for both states. No more calculations are given at lower electron energies because the Born approximation is not applicable for such scattering calculation here [17,46,58]. So we use the "MRD-CI (BE-scaled)" results in the energy range from thresholds to 5 keV as the present theoretical calculations to compare with the previous results in Sec. IV.

IV. RESULTS AND DISCUSSION

A. The GOSs for $\tilde{A}^1B_1$ and $\tilde{B}^1A_1$ of H_2O

Figures 4(a) and 4(b) show the present experimental and theoretical (labeled as "MRD-CI") GOSs for $\tilde{A}^1B_1$ and $\tilde{B}^1A_1$ of H_2O, respectively, together with the previous experimental and theoretical results. Figure 4(a) shows the present GOSs of $\tilde{A}^1B_1$ are in excellent agreement with the ones measured
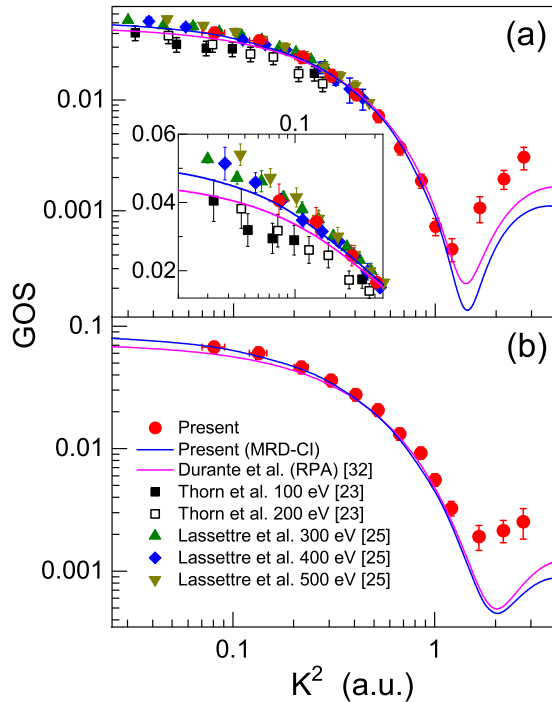
FIG. 4. The GOSs for (a) $\tilde{A}^1B_1$ and (b) $\tilde{B}^1A_1$, in comparison to different experimental results and calculations (see text for details).

FIG. 5. The OOSs for (a) $\tilde{A}^1B_1$ and (b) $\tilde{B}^1A_1$, along with previous measurements and calculations. Experiments: 1 present, 2 Thorn *et al.* [23], 3 Lassettre *et al.* [25], 4 Chan *et al.* [56], 5 Yoshino *et al.* [68], 6 Lee and Suto [69], 7 Laufer and McNesby [70], 8 Harrison *et al.* [65], 9 Watanabe and Zelikoff [71]. Theories: 10 present, 11 Durante *et al.* [32], 12 Bhanuprakash *et al.* [37], 13 Phillips and Buenker [66], 14 Theodorakopoulos *et al.* [72], 15 Buenker and Peyerimhoff [75], 16 Nicolaides *et al.* [76], 17 Wood [77], 18 Williams and Langhoff [74], 19 Rauk and Barriel [73], and 20 Yeager *et al.* [67]. Shadow areas show error bar ranges of the present two OOSs.

by Lassettre *et al.* at $E_0 = 300$–500 eV [25], and in rough shape agreement, but consistently higher than the ones of Thorn *et al.* at $E_0 = 100$ and 200 eV (25% on average) [23]. This difference could be attributed to the spectral fitting errors of Thorn *et al.* [23] as discussed above. Our GOSs are in very good agreement with our MRD-CI calculation, and in reasonable agreement with the random phase approximation (RPA) theory of Durante *et al.* [32] within the FBA in $K^2 < 1.2$ a.u., while are much higher than both calculations in $K^2 > 1.2$ a.u., which is well known to be due to the invalidity of the FBA for large K^2 [17,46,58]. The second Born term within the Born approximation would contribute appreciably in large K^2, which should be introduced into the complicated scattering calculation, where all possible intermediate states should be included [17,46,58]. To the best of our knowledge, there are no available experimental GOSs compared for $\tilde{B}^1A_1$. Figure 4(b) shows our GOSs of $\tilde{B}^1A_1$ are in good agreement with our MRD-CI calculation, and in rough shape agreement, but consistently higher than the RPA calculation [32] by about 12% on average in $K^2 < 1.2$ a.u., while are largely higher than both calculations in $K^2 > 1.2$ a.u. with the same reason for $\tilde{A}^1B_1$. The differences of GOSs for both states between our MRD-CI calculations and RPA ones [32] in $K^2 < 0.3$ a.u. and $K^2 > 1.2$ a.u. should be due to the limited precision of the electronic wave functions in RPA [32], where an approximate treatment of the electron correlation effect was made by neglecting the contribution of some terms to optimize the calculation amount.

To confirm the reliability of the GOSs for $\tilde{A}^1B_1$ and $\tilde{B}^1A_1$, and to clarify the chaos of the early reported OOSs, the two OOSs derived from Eq. (3) are shown in Fig. 5 and compared to different experimental and theoretical results,
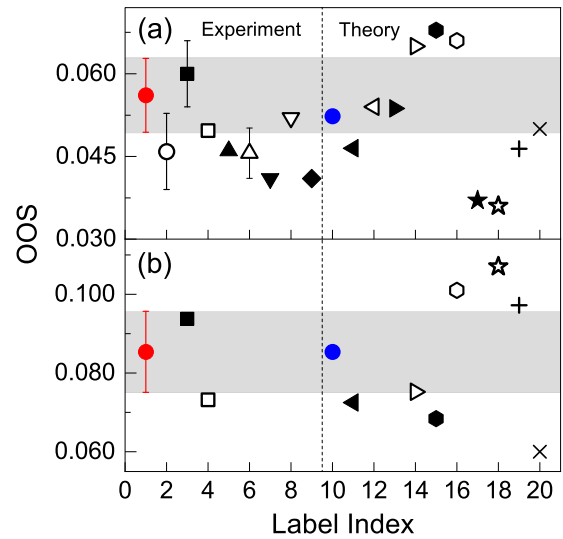
respectively. Figure 5(a) shows our OOS for $\tilde{A}^1B_1$ is in good agreement with the experimental ones of Lassettre *et al.* by EELS [25], Harrison *et al.* by photoabsorption [65] and Chan *et al.* by dipole(e, e) [56], and with the theoretical ones of Bhanuprakash *et al.* [37], Phillips *et al.* [66], and ours by MRD-CI and Yeager *et al.* by the equations-of-motion method [67]. The experimental results of Thorn *et al.* by EELS [23], Yoshino *et al.* [68] and Lee and Suto [69] by photoabsorption are in reasonable agreement with our OOS if considering the mutual experimental errors, while the results of Laufer and McNesby [70] and Watanabe and Zelikoff [71] by photoabsorption are underestimated, which could be limited by the poor experimental conditions at that time. Figure 5(b) shows our OOS for $\tilde{B}^1A_1$ is in good agreement with the measurements of Lassettre *et al.* by EELS [26] and Chan *et al.* by dipole(e, e) [56], and with the calculations of this work and Theodorakopoulos *et al.* [72] by MRD-CI, Rauk and Barriel by the perturbation theory [73] and Durante *et al.* by RPA [32]. The differences among our OOSs and the other theoretical results for both states could be limited by their calculation methods and basis sets for electronic wave functions [74–77] at that time. All above nicely supports the reliability and accuracy of our OOSs and GOSs.

B. The ICSs for $\tilde{A}^1B_1$ and $\tilde{B}^1A_1$ of H_2O

Since the reliable GOSs were obtained above, according to the Eqs. (3)–(6), the present BE-scaled ICSs for $\tilde{A}^1B_1$ and
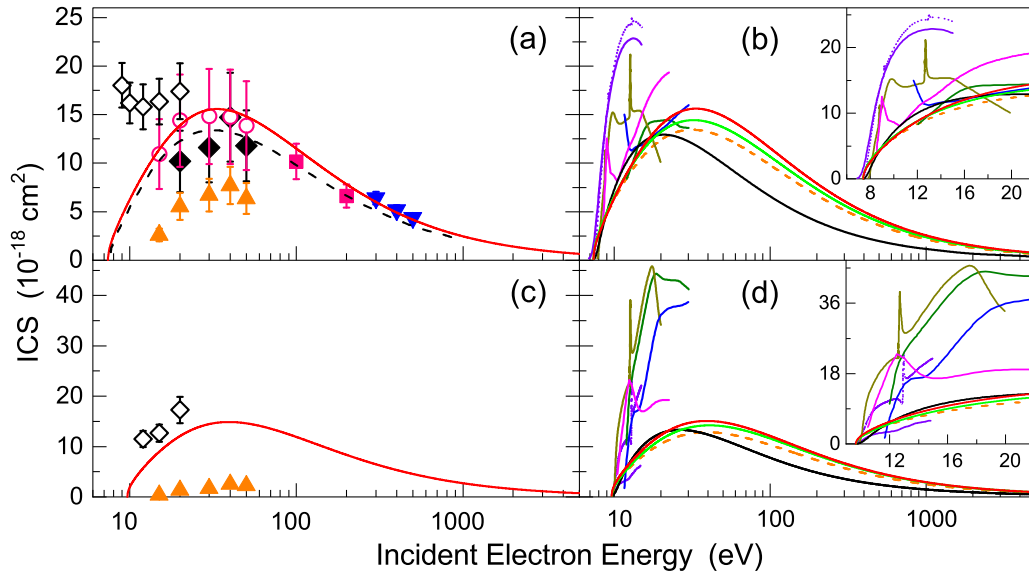
FIG. 6. The ICSs for (a, b) $\tilde{A}^1B_1$ and (c, d) $\tilde{B}^1A_1$, along with previous measurements and calculations. Experiments [(a) and (c)]: red solid line present (BE-scaled ICSs), black dashed line Matsui *et al.* (BEf-scaled ICSs) [18], filled inverted triangle Lassettre *et al.* [25], filled square Sophia University [23], open circle Matsui *et al.* [18], filled rhombus the combined data from Sophia and Flinders Universities [23], filled triangle Flinders University [23], open rhombus Ralphs *et al.* [19]. Theories [(b) and (d)]: green solid line present (MRD-CI), orange dashed line Durante *et al.* (RPA) [32], black solid line Kutcher *et al.* (ELF) [9,78], blue solid line Ralphs *et al.* (SMC) [19], magenta solid line Rescigno *et al.* (complex Kohn) [29], olive solid line Gil *et al.* (complex Kohn) [34], violet solid line Gorfinkiel *et al.* (*R*-matrix, ANA) [30], violet dotted line Gorfinkiel *et al.* (*R*-matrix, FNA) [30], and dark yellow solid line Morgan *et al.* (*R*-matrix) [31].

$\tilde{B}^1A_1$ of H_2O were derived and shown in Fig. 6, together with previous measurements and calculations. In Fig. 6(a), the present ICS for $\tilde{A}^1B_1$ is in excellent agreement with the experimental results of Lassettre *et al.* at $E_0 = 300$–500 eV [25] and Matsui *et al.* at $E_0 = 15$–50 eV [18], and is in reasonable agreement with the ones from Sophia University at $E_0 = 100$ and 200 eV (higher by 12%) [23], while is in shape agreement, but consistently slightly higher than the BEf-scaled ICS (15% on average) of Ref. [18]. It is easily understood for the slightly lower values of the BEf-scaled ICS of Ref. [18] since they used a lower OOS value of 0.0497 [56] to scale their ICS. Here Matsui *et al.* have carefully minimized the errors of the spectral fitting at low energies and the normalization procedure by a new approach [18]. In addition, our ICS is higher than the combined data from Flinders University and Sophia University at $E_0 = 20$–50 eV by 25% on average except the one at $E_0 = 40$ eV [23] and the independent data from Flinders University at $E_0 = 15$–50 eV by 60% on average [23], while is smaller than the ones of Ralphs *et al.* at $E_0 = 9$–20 eV by 20%–75% [19]. The big differences are due to the errors from the spectral fitting and the normalization procedure in the low-energy experiments [19,23] as discussed above. Theoretically, as shown in Fig. 6(b), our ICS is in good agreement with our MRD-CI calculation in the whole energy range, and the ones of Durante *et al.* at $E_0 < 15$ eV and $E_0 > 1000$ eV by RPA [32], Kutcher *et al.* at $E_0 < 15$ eV by the energy loss function model (ELF) [9,78], and Ralphs *et al.* at $E_0 = 12$–30 eV by the Schwinger multichannel method (SMC) [19], and is roughly comparable to Gil *et al.* at $E_0 = 12$–30 eV by the complex Kohn method [34], while is in large disagreement with them at the corresponding remaining

energy regions. The large discrepancies of our ICS with the *R*-matrix [30,31] and the complex Kohn calculations [29] may be due to the difficulties to capture the coupling between a number of relatively closely spaced states that have mixed valence-Rydberg character, and the use of correlated target wave functions in coupled-state calculations could introduce a set of problems associated with the appearance of unphysical pseudoresonances.

Figure 6(c) shows the present ICS for $\tilde{B}^1A_1$ is smaller than the experimental results of Ralphs *et al.* [19] by 35% on average, and is much larger than the ones of Flinders University [23]. Theoretically, as shown in Fig. 6(d), our ICS is in very good agreement with our MRD-CI calculation over the entire energy range, and the ones of Durante *et al.* at $E_0 < 13$ eV and $E_0 > 1000$ eV by RPA [32] and Kutcher *et al.* at $E_0 < 19$ eV by ELF [9,78], while is in large disagreement with them at the remaining energy regions. Moreover, our ICS is in rough sharp agreement with the *R*-matrix calculation in the ANA [30] with the maximum difference by about 36%, but is dramatically smaller than that in the FNA [30] and the other calculations [19,29,31,34]. The reasons for the disagreement of our ICSs for $\tilde{B}^1A_1$ with previous experiments and theories are similar with those for $\tilde{A}^1B_1$. Clearly, the excellent agreement of our ICSs for both excitations with the measurements of Lassettre *et al.* [23,25], Matsui *et al.* [18], Sophia University group at $E_0 = 100$–200 eV [23], and the present MRD-CI calculations strongly supports the high reliability and accuracy of present data, which could resolve the large differences of ICSs among experiments and theories for decades. In addition, the ICSs of Kutcher *et al.* by ELF [9,78] generally used in radiation track simulation codes

(e.g., KURBUC [7], RETRACKS [9], EPOTRAN [10]) should be revised.

V. CONCLUSIONS

With the aid of the BE-scaling approach, the BE-scaled ICSs for $\tilde{A}^1B_1$ and $\tilde{B}^1A_1$ of H_2O from excitation thresholds to 5 keV have been obtained using high-energy electron scattering for eliminating the spectral fitting errors in low-energy measurements, which could resolve the long-term controversy regarding the dramatic differences of ICSs among earlier experiments and theories by combing the present *ab initio* calculations. This work improves our knowledge of recommended cross sections for electron scattering from H_2O, which tremendously contributes to modeling interaction processes between electrons and water-containing systems in planetary atmospheres, plasmas, radiation chemistry and biology and biomedicine.

[1] L. Campbell and M. J. Brunger, Plasma Sources Sci. Technol. **22**, 013002 (2013).

[2] X. Ren, E. Wang, A. D. Skitnevskaya *et al.*, Nat. Phys. **14**, 1062 (2018).

[3] B. C. Garrett, D. A. Dixon, D. M. Camaioni *et al.*, Chem. Rev. **105**, 355 (2005).

[4] E. Alizadeh and L. Sanche, Chem. Rev. **112**, 5578 (2012).

[5] B. Boudaïffa, P. Cloutier, D. Hunting *et al.*, Science **287**, 1658 (2000).

[6] C. Champion, Phys. Med. Biol. **48**, 2147 (2003).

[7] H. Nikjoo, D. Emfetzoglou, T. Liamsuwan *et al.*, Rep. Prog. Phys. **79**, 116601 (2016).

[8] S. Incerti, I. Kyriakou, M. A. Bernal *et al.*, Med. Phys. **45**, e722 (2018).

[9] I. Plante and F. A. Cucinotta, New J. Phys. **11**, 063047 (2009).

[10] C. Champion, C. L. Loirec, and B. Stosic, Int. J. Rad. Bio. **88**, 54 (2012).

[11] W. Friedland, E. Schmitt, P. Kundrát *et al.*, Sci. Rep. **7**, 45161 (2017).

[12] A. Muñoz, F. Blanco, G. Garcia *et al.*, Int. J. Mass Spectrom. **277**, 175 (2008).

[13] Y. Itikawa and N. Mason, J. Phys. Chem. Ref. Data **34**, 1 (2005).

[14] J. de Urquijo, E. Basurto, A. M. Juárez *et al.*, J. Chem. Phys. **141**, 014308 (2014).

[15] D. Emfietzoglou, K. Karava, G. Papamichael *et al.*, Phys. Med. Biol. **48**, 2355 (2003).

[16] R. Signorell, Phys. Rev. Lett. **124**, 205501 (2020).

[17] H. Tanaka, M. J. Brunger, L. Campbell, H. Kato, M. Hoshino, and A.R. P. Rau, Rev. Mod. Phys. **88**, 025004 (2016).

[18] M. Matsui, M. Hoshino, H. Kato *et al.*, Eur. Phys. J. D **70**, 77 (2016).

[19] K. Ralphs, G. Serna, L. R. Hargreaves *et al.*, J. Phys. B: At. Mol. Opt. Phys. **46**, 125201 (2013).

[20] L. Hargreaves, K. Ralphs, G. Serna *et al.*, J. Phys. B: At. Mol. Opt. Phys. **45**, 201001 (2012).

[21] M. J. Brunger, P. A. Thorn, L. Campbell *et al.*, Int. J. Mass Spectrom. **271**, 80 (2008).

[22] P. A. Thorn, M. J. Brunger, H. Kato *et al.*, J. Phys. B: At. Mol. Opt. Phys. **40**, 697 (2007).

[23] P. A. Thorn, M. J. Brunger, P. J. O. Teubner *et al.*, J. Chem. Phys. **126**, 064306 (2007).

[24] K. N. Klump and E. N. Lassettre, Can. J. Phys. **53**, 1825 (1975).

[25] E. N. Lassettre and A. Skerbele, J. Chem. Phys. **60**, 2464 (1974).

[26] E. N. Lassettre and E. R. White, J. Chem. Phys. **60**, 2460 (1974).

[27] S. Trajmar, W. Williams, and A. Kuppermann, J. Chem. Phys. **58**, 2521 (1973).

[28] S. R. Mielczarek and K. J. Miller, Chem. Phys. Lett. **10**, 369 (1971).

[29] T. N. Rescigno and A. E. Orel, Phys. Rev. A **88**, 012703 (2013).

[30] J. D. Gorfinkiel, L. A. Morgan, and J. Tennyson, J. Phys. B: At. Mol. Opt. Phys. **35**, 543 (2002).

[31] L. A. Morgan, J. Phys. B: At. Mol. Opt. Phys. **31**, 5003 (1998).

[32] N. Durante, U. T. Lamanna, G. P. Arrighini *et al.*, Theor. Chim. Acta **90**, 115 (1995).

[33] M.-T. Lee, S. E. Michelin, T. Kroin *et al.*, J. Phys. B: At. Mol. Opt. Phys. **28**, 1859 (1995). M.-T. Lee, S. E. Michelin, L. E. Machado *et al.*, *ibid.* **26**, L203 (1993).

[34] T. J. Gil, T. N. Rescigno, C. W. McCurdy, and B. H. Lengsfield, Phys. Rev. A **49**, 2642 (1994).

[35] L. Chantranupong, G. Hirsch, R. J. Buenker *et al.*, Chem. Phys. **154**, 13 (1991).

[36] H. P. Pritchard, V. McKoy, and M. A. P. Lima, Phys. Rev. A **41**, 546(R) (1990).

[37] K. Bhanuprakash, P. Chandra, C. Chabalowski *et al.*, Chem. Phys. **138**, 215 (1989).

[38] K. J. Miller, S. R. Mielczarek, and M. Krauss, J. Chem. Phys. **51**, 26 (1969).

[39] Y.-K. Kim, M. Inokuti, G. E. Chamberlain *et al.*, Phys. Rev. Lett. **21**, 1146 (1968).

[40] H. Silva, J. Muse, M. C. A. Lopes, and M. A. Khakoo, Phys. Rev. Lett. **101**, 033201 (2008) and references therein.

[41] R. F. da Costa, M. T. do N. Varella, M. H. F. Bettega *et al.*, J. Chem. Phys. **144**, 124310 (2016); A. G. Falkowski, M. A. P. Lima, and F. Kossoski, *ibid.* **152**, 244302 (2020).

[42] F. A. Gianturco and A. Jain, Phys. Rep. **143**, 347 (1986); F. A. Gianturco, S. Meloni, P. Paioletti *et al.*, J. Chem. Phys. **108**, 4002 (1998); M. A. Khakoo, J. Blumer, K. Keane *et al.*, Phys. Rev. A **77**, 042705 (2008); T. N. Rescigno and B. I. Schneider, *ibid.* **45**, 2894 (1992).

[43] X. J. Liu, L. F. Zhu, X. M. Jiang *et al.*, Rev. Sci. Instrum. **72**, 3357 (2001).

[44] J. C. Nickel, P. W. Zetner, G. Shen, and S. Trajmar, J. Phys. E: Sci. Instrum. **22**, 730 (1989); Y. W. Liu, L. Q. Xu, D. D. Ni *et al.*, J. Geophys. Res., [Space Phys.] **122**, 3459 (2017).

[45] K. Z. Xu, R. F. Feng, S. L. Wu *et al.*, Phys. Rev. A **53**, 3081 (1996); N. M. Cann and A. J. Thakkar, J. Electron. Spectrosc. Relat. Phenom. **123**, 143 (2002); X. Y. Han and J. M. Li, Phys. Rev. A **74**, 062711 (2006); B. P. Xie, L. F. Zhu, K. Yang *et al.*, *ibid.* **82**, 032501 (2010).

[46] M. Inokuti, Rev. Mod. Phys. **43**, 297 (1971).

[47] E. N. Lassettre, J. Chem. Phys. **43**, 4479 (1965).

[48] K. N. Klump and E. N. Lassettre, J. Chem. Phys. **68**, 886 (1978).

[49] A. R. P. Rau and U. Fano, Phys. Rev. **162**, 68 (1967).

[50] L. Vriens, Phys. Rev. **160**, 100 (1967).

[51] Y. K. Kim, J. Chem. Phys. **126**, 064305 (2007).

[52] H. Kawahara, D. Suzuki, H. Kato, M. Hoshino, and H. Tanaka, J. Chem. Phys. **131**, 114307 (2009); Y. Y. Wang, J. M. Sun, and L. F. Zhu, *ibid.* **132**, 124301 (2010); Y.-W. Liu, L.-Q. Xu, T. Chen, D.-G. Qi, T. Xiong, and L.-F. Zhu, Astrophys. J. Suppl. Ser. **234**, 10 (2018); L. Q. Xu, X. Kang, Y. G. Peng *et al.*, Phys. Rev. A **97**, 03250 (2018).

[53] Y. K. Kim, Phys. Rev. A **64**, 032713 (2001) and references therein.

[54] R. Mota, R. Parafita, A. Giuliani *et al.*, Chem. Phys. Lett. **416**, 152 (2005).

[55] W. A. Goddard, III and W. J. Hunt, Chem. Phys. Lett. **24**, 464 (1974).

[56] W. F. Chan, G. Cooper, and C. E. Brion, Chem. Phys. **178**, 387 (1993).

[57] R. J. Buenker, M. Honigmann, and H.-P. Liebermann, J. Chem. Phys. **113**, 1046 (2000); L.-Q. Xu, X. Kang, Y.-G. Peng *et al.*, Phys. Rev. A **97**, 032503 (2018).

[58] B. H. Bransden and C. J. Joachain, Physics of Atoms and Molecules (Prentice Hall, Harlow, UK, 2003); P. G. Burke, in *Atomic and Molecular Data and their Application: ICAMDATA Second International Conference*, edited by K. A. Berrington and K. L. Bell, AIP Proc. Conf. No. 543 (AIP, New York, 2000).

[59] T. H. Dunning, J. Chem. Phys. **90**, 1007 (1989).

[60] H.-J. Werner, P. J. Knowles, G. Knizia, F. R. Manby, and M. Schütz, WIREs Comput. Mol. Sci. **2**, 242 (2012).

[61] Q. Ma and H. Werner, WIREs Comput. Mol. Sci. **8**, e1371 (2018).

[62] R. J. Buenker and S. D. Peyerimhoff, Theor. Chim. Acta **35**, 33 (1974).

[63] R. J. Buenker and S. D. Peyerimhoff, Theor. Chim. Acta **39**, 217 (1975).

[64] R. J. Buenker, S. D. Peyerimhoff, and W. Butscher, Mol. Phys. **35**, 771 (1978).

[65] A. J. Harrison, B. J. Cederholm, and M. A. Terwilliger, J. Chem. Phys. **30**, 355 (1959).

[66] R. A. Phillips and R. J. Buenker, Chem. Phys. Lett. **137**, 157 (1987).

[67] D. Yeager, V. McKoy, and G. A. Segal, J. Chem. Phys. **61**, 755 (1974).

[68] K. Yoshino, J. R. Esmond, W. H. Parkinson *et al.*, Chem. Phys. **211**, 387 (1996).

[69] L. C. Lee and M. Suto, Chem. Phys. **110**, 161 (1986).

[70] A. H. Laufer and J. R. McNesby, Can. J. Chem. **43**, 3487 (1965).

[71] K. Watanabe and M. Zelikoff, J. Opt. Soc. Am. **43**, 753 (1953).

[72] G. Theodorakopoulos, I. D. Petsalakis, C. A. Nicolaides *et al.*, Chem. Phys. **100**, 331 (1985); J. Chem. Phys. **82**, 912 (1985).

[73] A. Rauk and J. M. Barriel, Chem. Phys. **25**, 409 (1977).

[74] G. R. J. Williams and P. W. Langhoff, Chem. Phys. Lett. **60**, 201 (1979).

[75] R. J. Buenker and S. D. Peyerimhoff, Chem. Phys. Lett. **29**, 253 (1974).

[76] C. A. Nicolaides and G. Theodorakopoulos, Int. J. Quantum Chem., Quantum Chem. Symp. **14**, 315 (1980).

[77] M. H. Wood, Chem. Phys. Lett. **28**, 477 (1974).

[78] G. J. Kutcher and A. E. S. Green, Rad. Res. **67**, 408 (1976).